How to cite: Angew. Chem. Int. Ed. 2025, e202418146
doi.org/10.1002/anie.202418146

NMR Spectroscopy

Ultrasensitive Characterization of Native Bacterial Biofilms via Dynamic Nuclear Polarization-Enhanced Solid-State NMR

*Chang-Hyeock Byeon, Ted Kinney, Hakan Saricayir, Kasper Holst Hansen, Faith J. Scott, Sadhana Srinivasa, Meghan K. Wells, Frederic Mentink-Vigier, Wook Kim, and Ümit Akbey**

Abstract: Bacterial biofilms are major contributors to persistent infections and antimicrobial resistance, posing significant challenges to treatment. However, obtaining high-resolution structural information on native bacterial biofilms has remained elusive due to the methodological limitations associated with analyzing complex biological samples. Solid-state NMR (ssNMR) has shown promise in this regard, but its conventional application is hindered by sensitivity constraints for unlabeled samples. In this study, we utilized high-sensitivity Dynamic Nuclear Polarization (DNP) ssNMR to characterize native *Pseudomonas fluorescens* colony biofilms. The ~75-fold sensitivity enhancement provided by DNP enabled structural characterization without isotope labeling or chemical/physical modification. We successfully collected 1D $^{13}C/^{15}N$, and 2D ^{1}H–^{13}C, ^{1}H–^{15}N and ^{13}C–^{13}C ssNMR spectra within seconds, minutes or hours, facilitating the identification and quantification of biofilm extracellular matrix (ECM) components. Additionally, DNP ssNMR allowed quantitative detection of both flexible and rigid biofilm components by favorable freezing conditions. This study represents the first application of ultrasensitive DNP ssNMR to characterize a native bacterial biofilm, significantly expanding the capabilities of ssNMR for analyzing the composition and structure of a wide array of *in vitro* and *ex vivo* biofilms. The versatility of this approach will accelerate structure-guided efforts to combat infections caused by biofilm-forming microbes.

Introduction

Bacteria form structured communities known as biofilms, which provide a protective environment against various stressors. Biofilm-associated bacteria account for approximately 80 % of chronic infections[1] and play a significantly role in the growing threat of antimicrobial resistance (AMR).[2] Within biofilms, bacterial cells exhibit antibiotic tolerance levels several orders of magnitude higher than their planktonic counterparts.[3] AMR-related diseases cause around one million deaths annually and are projected to surpass cancer as the leading cause of death by 2050.[4] Effectively combatting biofilm mediated infections and AMR necessitates the development of innovative therapeutic strategies targeting the structural components of biofilms.[5]

The structural integrity of biofilms relies on a complex extracellular matrix (ECM) that surrounds bacterial cells. This ECM is composed of polymeric fibrillar functional amyloids, polysaccharides, lipids, extracellular DNA (eDNA), and various metabolites.[6] Disrupting key structural components within biofilms, such as functional amyloids or polysaccharides, destabilizes biofilms and renders the encased bacteria more susceptible to drug interventions.[7] Despite their critical role, structural information on these components remains limited. For example, only a few structures are available for the biofilm forming cross-β functional bacterial amyloids (FuBA): the low-resolution structure of CsgA from *E. coli* and the high-resolution structures of TasA from *B. subtilis* and PSMα1 from *S. aureus*, the latter two determined in part by our group[8] Similarly, high-resolution structural data on the biofilm ECM polysaccharides remain scarce.[9]

Analyzing the structure of biological compounds within their native physiological environments poses significant

[*] C.-H. Byeon, T. Kinney, Dr. H. Saricayir, K. Holst Hansen, Prof. Ü. Akbey
Department of Structural Biology, School of Medicine, University of Pittsburgh, Pittsburgh, PA 15261, USA
E-mail: umitakbey@pitt.edu
K. Holst Hansen
Department of Biomedicine, Aarhus University, Aarhus 8000, Denmark
Dr. F. J. Scott, Dr. F. Mentink-Vigier
National High Magnetic Field Laboratory, Florida State University, Tallahassee, FL 32310, USA
S. Srinivasa, M. K. Wells, Prof. W. Kim
Department of Biological Sciences, Duquesne University, Pittsburgh, PA 15282, USA
Dr. F. Mentink-Vigier
Department of Chemistry and Biochemistry Florida State University Tallahassee, FL 32306, USA

technical challenges.[10] High-resolution techniques such as NMR spectroscopy and cryo-electron microscopy (EM) or tomography show great promise for studying these complex biological systems.[10,11] Among these, NMR spectroscopy stands out due to its ability of providing a comprehensive, quantitative overview of a biofilm sample. However, the complexity of biomolecules in native environments often requires multidimensional (nD) NMR methods to resolve and simplify overlapping signals. Effective analysis typically relies on isotopic enrichment at high concentrations, which is impractical for native samples like patient-derived biofilms, such as those from cystic fibrosis.[12] Magic-angle spinning (MAS) ssNMR (ssNMR) can deliver high-resolution structural insights into insoluble species, but its low sensitivity remains limiting, in particular for unlabeled native biofilms. Enhancing sensitivity is therefore imperative for rapid and effective ssNMR analysis of such biological native samples. Dynamic nuclear polarization enhanced ssNMR (DNP ssNMR) addresses this sensitivity issue, enabling characterization of native systems.[13]

Over the past decade, ssNMR has been utilized to analyze the chemical composition of diverse biological samples, including bacterial, plant, and fungal cell walls. However, these studies predominantly employed 1D ssNMR spectroscopy,[13k,14] which limits accurate quantification due to inherent low resolution and signal overlap. Nonetheless, valuable insights into the structure and composition of bacterial and fungal biofilms were obtained.[14–15] Multidimensional (nD) ssNMR, particularly 2D ssNMR, overcomes these limitations associated with 1D ssNMR spectroscopy, enabling the differentiation of signals originating from distinct components within complex biological mixtures. Specifically, 2D ^{13}C-^{13}C ssNMR requires either isotope labelling or sensitivity-enhancement through techniques like DNP. While a few studies have applied 2D ssNMR to plant and fungal cell walls with or without DNP,[16] examples in bacterial systems remain limited. To date, nD ssNMR has been applied to isotope-labeled or natural abundance whole bacteria and extracted pure cell walls.[17] High-resolution proton or carbon detected ssNMR techniques have also been employed in investigations of bacterial and plant cell walls.[17b,c,18] Recently, we and others demonstrated 2D ^{1}H-^{13}C ssNMR using proton or carbon detection in non-tuberculous mycobacteria (NTM) and *Pseudomonas fluorescens*.[17d,19] Furthermore, DNP ssNMR has been applied to characterize whole-cell and extracted cell walls from bacteria and yeast.[13k,17a,b,18,20]

In previous studies, we employed conventional room-temperature 1D and 2D ssNMR spectroscopy to analyze colony biofilms of *P. fluorescens* Pf0-1 and planktonic nontuberculous mycobacteria (NTM) at natural abundance.[19,21] Building on this foundation, here in this study we present the use of ultrasensitive 1D and 2D DNP ssNMR to characterize native colony biofilms of *P. fluorescens* Pf0-1. This biofilm model system is advantageous due to its diverse ECM components and non-pathogenic nature, enabling safe laboratory experimentation. Our findings demonstrate the potential of DNP ssNMR to rapidly acquire high-sensitivity 1D ssNMR spectra within seconds or minutes and 2D ssNMR spectra within hours, from native, natural abundance bacterial biofilm. By combining ^{13}C detection with 2D spectroscopy, we achieved enhanced spectral resolution, enabling quantification of biofilm components, and discovery of new structural insights. Operating at low temperature (~100 K), DNP ssNMR simultaneous captures both rigid and mobile ^{13}C signals, facilitating comprehensive quantitative signal detection. To the best of our knowledge, this study is the first demonstration of sensitivity-enhanced DNP ssNMR for intact native bacterial biofilm characterization. The experimental pipeline outlined here pushes the boundaries of NMR-based biofilm research and offers adaptability to various biofilm preparations and model systems. This advancement paves the way for structural studies of biofilms with unprecedented sensitivity and detail.

Results and Discussion

Structural Characterization of Native Bacterial Biofilm with Hyperpolarized DNP ssNMR

Biofilm samples for ssNMR analysis were prepared using two different methods, as illustrated in Figure 1. First, the native wet *P. fluorescens* colony biofilm was analyzed without any treatment, referred to as the 'wet biofilm'. This sample serves as a reference, preserving the natural water content of the biofilm. Second, the biofilm was gently dried at 50 °C, referred to as the 'dry biofilm'. Drying effectively removed excess hydration, significantly increasing sample packing efficiency and improving sensitivity by approximately tenfold. The CP-based spectra of the wet and dry biofilm samples, shown in Figures 2A,B, revealed minimal

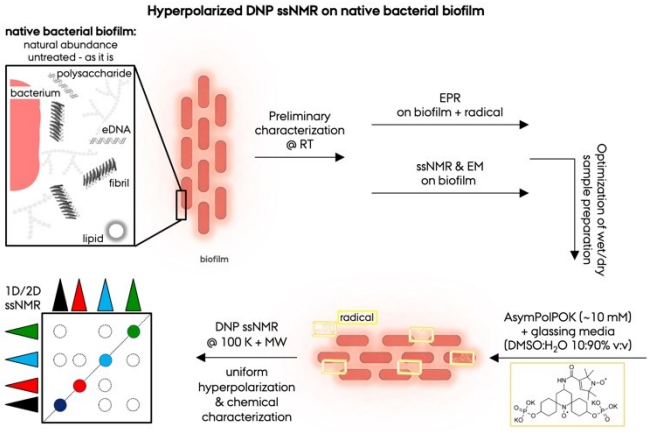

Figure 1. Experimental protocol for the hyperpolarized DNP NMR based structural characterization of native bacterial biofilms. The cartoon representation of essential structural components of biofilm such as polysaccharides, fibrillar functional amyloid proteins, eDNA and lipids. From the native biofilm sample preparation towards the final ssNMR spectrum. Experimental conditions require careful optimization to maximize the sensitivity and reproducibility by including MAS NMR and EPR characterization.

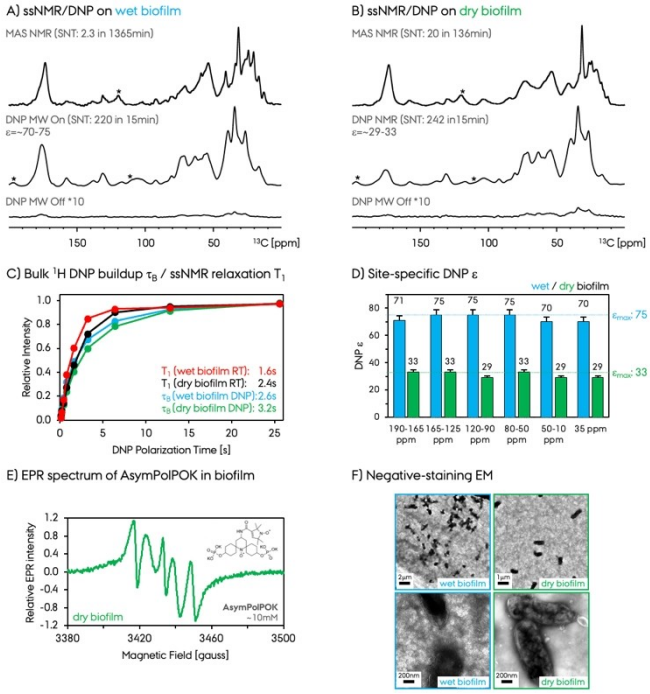

Figure 2. The 1D ^{13}C CP spectra were recorded with conventional ssNMR at ~300 K, 10 kHz and 750 MHz magnet, and the high-sensitivity DNP-enhanced ssNMR at ~100 K, 10 kHz and at 600 MHz magnet on A) wet (native) and B) dry biofilm preparations. The signal to noise ratio per root unit time (SNT, determined by (S/N)/(minute$^{0.5}$)) values in terms of min$^{-1/2}$ are given for a direct sensitivity comparison along with the total experiment times. For the DNP ssNMR spectra the μw on and off spectra are shown. The maximum DNP enhancements for the wet and dry biofilm samples are ε: ~75 and ~33, respectively. C) The DNP buildup times (τ_B) and the ssNMR relaxation times (T_1) are recorded by saturation-recovery method. The normalization was done at 52.8 s to 1.0 for each data set separately. D) Site-specific DNP ε for wet and dry biofilm samples. 190–165 ppm indicates CO signals, 165–125 ppm aromatic and nucleic acids, 120–90 ppm polysaccharides, 80–50 ppm polysaccharides and Cα, 50–10 ppm Cα and aliphatics, and ~35 ppm lipids. Error bars represent a constant 5% error. E) The EPR spectrum of the freshly prepared dry biofilm sample containing 10 mM AsymPol-POK radical recorded at room temperature right before performing the DNP experiment. The ^{13}C peaks at ~119.7 ppm for room-temperature spectra and ~111.4 ppm for DNP spectra are spinning sidebands and marked with asterisks. F) The negative-staining EM micrographs of the wet and dry biofilm samples. The scale bar is 200 nm and 1/2 μm.

differences, consistent with previous findings using conventional ssNMR methods.[19b] Small intensity changes between the wet and dry samples are likely due to variations in sample dynamics and CP efficiency. These observations suggest that the drying process did not alter the biofilm's chemical composition.

Both wet and dry biofilm samples were incubated with a radical for DNP hyperpolarization and measured at ~100 K under μw irradiation, Figure 1. The AsymPol-POK radical, dissolved in a DMSO/water (10:90 % v:v) DNP buffer, was employed as the polarization agent. This radical has demonstrated high efficiency at higher magnetic fields and exhibited short polarization buildup times at 10 mM concentration. The results of ssNMR and EPR characterizations are presented in Figure 2A-E. Additionally, the EM micrographs of the wet and dry biofilm samples were recorded prior to the radical incubation. The micrographs confirm the presence of intact bacteria surrounded by ECM, Figure 2F. The majority of the biofilm's mass is composed of ECM, with bacterial signals contributing only a small fraction.

DNP hyperpolarization resulted in a significant signal enhancement of ε:~75 for the wet biofilm preparation in the ^{13}C CP DNP ssNMR spectra, Figure 2A. This represents one of the highest DNP enhancements observed among various native biological sample preparations on a 600 MHz DNP system. In comparison, previous studies have reported DNP enhancements of ε:~45–60 for whole cell preparations at 600 MHz, ε:~25 for drugs inside intact cells at 400 MHz, ε:~30 for cell wall of whole or disrupted bacteria at 400 MHz, and ε:~30 for fungi and plant samples. Notably, the glycerol and/or polysaccharide fraction of *Aspergillus fumigatus* fungus exhibited a larger enhancement of ε:~90 at 600 MHz.[13i,20a,22]

For the dried biofilm preparation, protocol with impregnation resulted in a smaller enhancement of ε:~33 with a longer DNP buildup time, Figure 2B-D. These differences are attributed to a non-uniform and suboptimal biradical distribution and potentially increased microwave absorption by the sample. Furthermore, a decay in DNP enhancement was observed during prolonged incubation at room temperature (data not shown), suggesting deactivation or degradation of the radical within the native biofilm's reducing ECM environment. This was corroborated by EPR spectra, which revealed deactivated AsymPol-POK after extended incubation times, Figure S1. A similar phenomenon has been reported in previous *ex vivo* DNP studies on mammalian cells.[23] To mitigate this issue, all data presented in this study were acquired from freshly prepared biofilm samples and measured immediately.

The significant signal enhancements achieved confirm the immense potential of DNP ssNMR for characterizing native biofilms. The acquisition of 1D ^{13}C ssNMR spectra is completed within seconds to minutes using DNP ssNMR, offering sensitivity levels comparable to those that would typically require hours to days with conventional ssNMR, Figure 2A,B. The observed signal enhancement of ε:~33 and ~75 correspond to approximately 1000-fold (33^2) or 5625-fold (75^2) reduction in experimental time, respectively. Notably, the higher packing efficiency of the dry biofilm sample results in increased sensitivity despite a lower DNP enhancement. For the wet biofilm sample, a SNT: 220 min$^{-1/2}$ is achieved with 1D ^{13}C CP DNP ssNMR, representing a ~100-fold improvement over conventional room temperature spectra, Figure 2A. Similarly, for the dry biofilm sample, a SNT: 242 min $^{-1/2}$ is achieved, representing ~12-fold improvement over conventional CP ssNMR spectra, albeit with a lower enhancement, Figure 2B.

Bulk proton DNP buildup times (τ_B) were measured under μw irradiation at 100 K for both biofilm preparations and compared to bulk proton T_1 relaxation times recorded at ~300 K, Figure 2C. The τ_B values are only slightly longer than the room temperature T_1 values due to the favorable

rapid polarization buildup properties of the AsymPol-POK radical.[24] The electron paramagnetic resonance (EPR) spectrum of AsymPol-POK in freshly prepared native wet biofilm sample is presented in Figure 2E. These relatively short τ_B times significantly improve overall SNT, particularly when contrasted with longer buildup times observed when using different radicals, such as AMUPOL.[25] The dry biofilm sample exhibited longer τ_B/T_1 ratios compared to the wet sample. Interestingly, the proton τ_B values were consistent across different chemical sites (Figure S2), indicating a uniform distribution of the radical within the biofilm, which facilitates quantitative characterization, Figure 2D. Uniform DNP enhancements of ε:70–75 for the wet sample and ε:29–33 for the dry sample were observed across various chemical sites, Figure S3.[19b] This contrasts with previous DNP ssNMR studies of complex environments which reported site-specific ε values.[13i,20a,22]

To extend the chemical information, we recorded a high-sensitivity ^{15}N CP DNP ssNMR spectrum of the native wet biofilm sample, Figure 3, in ~35 min, achieving a SNT:11 min$^{-1/2}$. For comparison, the conventional ^{15}N CP spectrum recorded at room temperature from a fully packed biofilm sample is shown in Figure S4. This spectrum recorded in 273 min to achieve a SNT:~0.24 min$^{-1/2}$, highlighting a ~50-fold sensitivity increase with DNP ssNMR. Tentative resonance assignments in the 1D ^{13}C/ ^{15}N DNP ssNMR spectrum are shown in Figure 3B.[26]

The ^{13}C FWHM linewidths of ~185 Hz (~1 ppm) and ~490 Hz (~2.6 ppm) were observed at room temperature experiments for wet *Pseudomonas* biofilm sample, based on INEPT and CP ssNMR, respectively, using a 750 MHz ssNMR system.[19] The room-temperature 1D ^{13}C CP ssNMR spectra for both wet and dry biofilm samples are shown in Figure 2A,B. Remarkably, lowering the experimental temperature from 300 K to 100 K produced ^{13}C CP spectra with similar overall resolution. Spectrum deconvolution indicates ~30% resonance broadening at DNP ssNMR spectra at ~100 K, with average linewidths of ~640 Hz (~4.3 ppm) and ~380 Hz (~6.3 ppm) for ^{13}C and ^{15}N spectra recorded, respectively, Figure 3 and Table 1.

High-Throughput Biofilm Compositional Analysis

The peak deconvolution of the 1D DNP ssNMR spectra identified 38 and 19 resonances for tentative assignments from the ^{13}C and ^{15}N CP spectra, respectively, Figure 3. This is slightly fewer than the 59 peaks observed at the room temperature spectra due to broadening of the resonances at ~100 K. While tedious and time consuming, peak deconvolution provides a critical foundation for resonance and chemical shift identification. Correlated with the 2D ^{1}H-^{13}C and ^{1}H-^{15}N DNP ssNMR spectra shown in Figure 5, these peaks align with the presence of proteins, polysaccharides and other species as previously observed, Figure 3C.[28] Following our recent room temperature biofilm study,[19] ^{13}C signals were assigned to: aliphatic carbons (proteins, carbohydrates, and lipids) at ~10–50 ppm, glycine Cα at ~45 ppm, peptide/protein Cα/Cβ at ~50–70 ppm, polysaccharides at ~65–110 ppm, aromatic signals (proteins/nucleic acids) at ~110–165 ppm, and CO (carbonyl/carboxyl) at ~165–190 ppm, Figures 2,3.

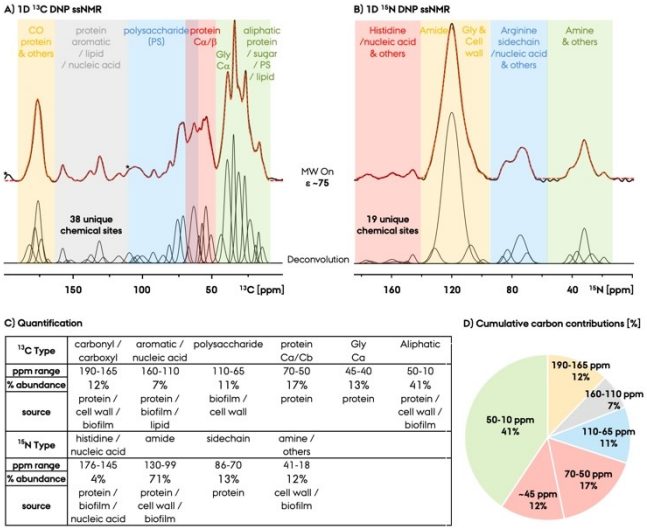

C) Quantification

^{13}C Type	carbonyl / carboxyl	aromatic / nucleic acid	polysaccharide	protein Cα/Cb	Gly Cα	Aliphatic
ppm range	190-165	160-110	110-65	70-50	45-40	50-10
% abundance	12%	7%	11%	17%	13%	41%
source	protein / cell wall / biofilm	protein / biofilm / lipid	biofilm / cell wall	protein	protein	protein / cell wall / biofilm
^{15}N Type	histidine / nucleic acid	amide	sidechain	amine / others		
ppm range	176-145	130-99	86-70	41-18		
% abundance	4%	71%	13%	12%		
source	protein / biofilm / nucleic acid	protein / cell wall / biofilm	protein	cell wall / biofilm		

Figure 3. Quantification of different chemical sites in the A) ^{13}C and B) ^{15}N CP DNP ssNMR spectra of natural abundance native wet bacterial biofilm. The long (1.2 ms for ^{13}C and 0.4 ms for ^{15}N) CP was used to ensure quantitative analysis. The individual peaks are determined by peak deconvolution utilizing ssNake program.[27] The list of these peaks along with their linewidths are given in Table 1. Different tentative group assignments are color coded and labelled. The ^{13}C peaks at ~111.4 and ~197 ppm are spinning sidebands and marked with asterisks in A. See Figure S1 for 1D ^{13}C DNP ssNMR at different MAS.

Table 1: List of signals determined by deconvolution of the ^{13}C and ^{15}N CP DNP NMR spectra of native wet bacterial biofilm shown in Figure 2A,B. Chemical shifts, relative integral ratios normalized to the maximum integral (bold number as 1.00) within the ^{13}C or ^{15}N peak lists. The linewidths and the tentative resonance assignments are given for ^{15}N resonances. The average full-width at half maximum, FWHM, for ^{13}C and ^{15}N signals are ~640 Hz (~4.3 ppm) and ~380 Hz (~6.3 ppm), respectively, with the processing parameters given in the methods section. The spectra were recorded on a 600 MHz NMR spectrometer. The asterisk indicates signals due to spinning sideband.

^{13}C CP						^{15}N CP		
ppm	rel. %	FWHM [Hz]	ppm	%	FWHM [Hz]	ppm	rel. %	FWHM [Hz]
15.4	0.12	571	93.8	0.18	650	18.5	0.01	245
18.0	0.15	370	102.1	0.09	984	26.7	0.03	389
20.1	0.09	371	105.5	0.08	766	31.5	0.11	347
24.2	0.45	807	108.0	0.04	580	36.4	0.03	319
28.0	0.56	499	111.4*	0.11	790	41.0	0.02	266
32.4	0.84	722	119.0	0.08	883	69.5	0.03	336
36.0	0.69	418	128.4	0.05	669	74.0	0.14	557
40.5	**1.00**	754	131.3	0.20	664	82.6	0.04	341
45.0	0.30	814	137.4	0.08	671	85.7	0.01	226
52.2	0.23	636	140.4	0.03	702	98.8	0.01	267
55.9	0.42	585	151.9	0.02	599	107.5	0.11	557
58.6	0.21	411	154.7	0.02	456	119.6	**1.00**	745
60.9	0.13	363	157.7	0.11	546	129.7	0.10	476
64.6	0.65	888	160.4	0.01	411	145.5	0.02	253
68.4	0.10	460	168.0*	0.02	435	149.3	0.01	169
72.3	0.43	704	172.9	0.19	690	154.8	0.01	618
76.2	0.42	749	175.2	0.57	810	159.3	0.02	417
82.2	0.12	512	177.5	0.29	720	173.3	0.01	322
86.6	0.07	700	181.5*	0.19	938	176.2	0.01	320

To further quantify biofilm components, deconvolution analysis of the CO ^{13}C signal (165–190 ppm) was performed for the dry and wet biofilm samples using conventional and DNP ssNMR spectra, Figure 4. Three distinct chemical sites were identified: 172.9, 175.2 and 177.5 ppm, consistent with previously assignments for bacterial cell-walls.[17c,28a,b,29] Peaks at 168.0 and 181.5 ppm are due to spinning sidebands.

The 172.9 ppm signal was assigned to protein "carbonyl site #1" and polysaccharides "ester sites" from the cell-wall/biofilm. Although 172.9 ppm resonance was previously associated with teichoic acid esters, Gram-negative *P. fluorescens* lacks teichoic and lipoteichoic acid. The 175.2 ppm signal was attributed to protein "carbonyl site #2", primarily from the biofilm and peptidoglycan peptides. The 177.5 ppm signal was assigned to "carboxyl signals" from uncross-linked ends of the cell wall peptidoglycans.

The 2D ^{1}H-^{13}C DNP ssNMR spectrum of the wet sample supports these resonance assignments, Figure 4E,5 showing proton correlations with CO signals deconvoluted in Figure 4A-D. Observed proton chemical shifts include amides at ~8–10 ppm, aromatics at ~6–7 ppm, nucleic acids at ~5 ppm, alpha at ~4.5 ppm, carbohydrate ring at ~4 ppm, and aliphatic at ~1–3 ppm. The 2D ^{1}H-^{13}C DNP ssNMR spectrum recorded with short CP (100 µs) primarily monitors directly bonded proton-carbon pairs.

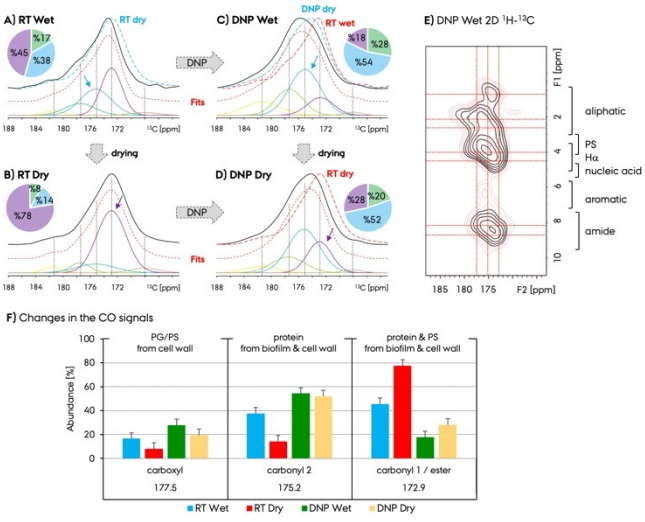

Figure 4. Quantification of the CO regions of the ^{13}C CP spectra recorded with A,B) conventional ssNMR at ~300 K and C,D) DNP ssNMR at ~100 K. The CO signals for the ^{13}C spectrum recorded for the A,C) wet and B,D) dry biofilm sample. E) The zoomed CO region of the 2D ^{1}H-^{13}C DNP ssNMR spectrum of the wet biofilm sample recorded with 100 µs CP contact time. F) The quantification of the three CO signals observed in the deconvolution analysis for wet/dry biofilm samples with constant 5% error bars. In A-D, the sum of the deconvoluted signals, the fitted spectrum, are shown as the spectrum with red dashed lines. Dashed black lines are placed at the corresponding chemical shifts of these five resonances. For direct comparison of the wet and dry spectra, the spectra from B and D are shown in A and C as light blue spectra. As a note, the color coding of the deconvoluted peaks and the bars in the graph are not correlated. The peaks at 168 and 181.5 ppm are due to sidebands.

The 172.9 and 175.2 ppm peaks correlate with the amide at ~8 and alpha protons at ~4.5 ppm, as well as aliphatic protons. In contrast, the 177.5 ppm peak shows weaker amide proton cross peak but correlates with the carbohydrate (~4 ppm) aliphatic, and aromatic (~6 ppm) protons at lower contour levels (data not shown). In summary, the 172.9 and 175.2 ppm signals originate from protein and/or polysaccharide species, while the 177.5 ppm peak predominantly reflects cell wall peptidoglycans. Relative abundances shown in Figures 3D and 4F describe the native biofilm compositions.

The effect of drying the biofilm on the conventional and DNP ssNMR spectra were quantified by comparing the spectra in Figure 4A with 4B and Figure 4C with 4D. Drying the biofilm increases the 172.9 ppm peak relative to the others, rising from ~45% to ~78% in the conventional spectra and 18% to 28% in the DNP spectra. This change corresponds to a reduction in the 175.2 and 177.5 ppm peaks to approximately half of their original intensity. We speculate that this is due to changes in molecular dynamics (and thus CP efficiency), potentially indicating that the polysaccharides and proteins (predominantly polysaccharide) in the wet biofilm are more flexible. Drying likely makes these components more rigid, thereby enhancing their CP signals. The CO region of the DNP ssNMR spectra for dry and wet samples showed similar trends, with the dry samples displaying a decreased 172.9 ppm resonance compared to room temperature ssNMR spectra.

The ^{15}N CP DNP ssNMR spectrum of the native wet biofilm was analyzed for structural insights, Figure 3B. The amide backbone nitrogen signals, ~120 ppm, are the most abundant signal originating from proteins, polysaccharides or peptidoglycan nitrogen sites within the biofilm. These amide resonances accounted for 71% of the total nitrogen signal integrated area and were deconvoluted into three major resonances centered at ~107.5, ~119.6 and ~129.7 ppm, Figure 3B and Table 1. The signals at 107.5 and 129.7 ppm present ~8% and 9% of the amide nitrogens, respectively, while the dominant amide peak 119.6 ppm constitutes ~82% of the total. These three resonances were also observed in the 2D ^{1}H-^{15}N DNP ssNMR spectrum, see dashed lines in Figure 5C. The resonance at 129.7 ppm, compared to the major peak at 119.6 ppm, suggests amides

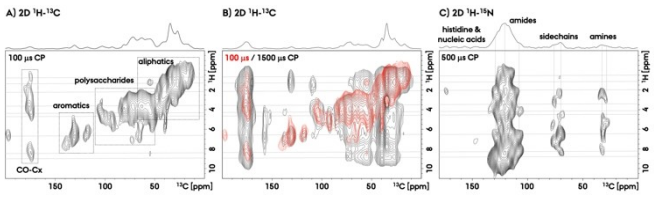

Figure 5. DNP-enhanced A,B) 2D ^{1}H-^{13}C and C) 2D ^{1}H-^{15}N FSLG HETCOR ssNMR spectra of natural abundance native wet bacterial biofilm. 100/1500 µs CP contact times were utilized. In B, the 2D spectrum with 100 µs contact time from A is shown in red, and the spectrum with 1500 µs is shown in black. The total experimental times are 18, 36 and 90 minutes for A, B and C, respectively.

in a distinct chemical environment, likely reflecting differences between biofilm and bacterial cell wall species.

Previous ssNMR studies of bacterial cell-wall and cell-wall-extract indicated two ^{15}N amide resonances: a less abundant peptidoglycan glycine at 107.5 ppm and a more abundant non-glycine amide from proteins at ~120 ppm.[30] In *S. aureus*, this glycine amide at 107.5 ppm accounted for ~17–28% of all amides.[30–31] In contrast, our study of the *P. fluorescens* biofilm sample shows a much lower abundance of ~8% for this signal. This reduced relative abundance of the cell-wall/peptidoglycan glycine resonance is consistent with the biofilm's extensive extracellular matrix surrounding the bacterial cells.

In addition to amide resonances, amine signals at 26.7–41 ppm and protein sidechain signals at 69.5–85.7 ppm were also observed, comprising 11 % and 13 % of the total nitrogen signals, respectively. Furthermore, resonances between 145–176 ppm (predominantly at ~145.5, ~159.3 and ~176.2 with minor peaks listed in Table 1) indicate histidine and/or nucleic acid nitrogen signals,[31] representing ~3 % of the total nitrogen signal. However, no proton correlations were observed for these cross-peaks in the 2D ^{1}H-^{15}N DNP ssNMR spectrum, likely due to their lower abundance and SNT.

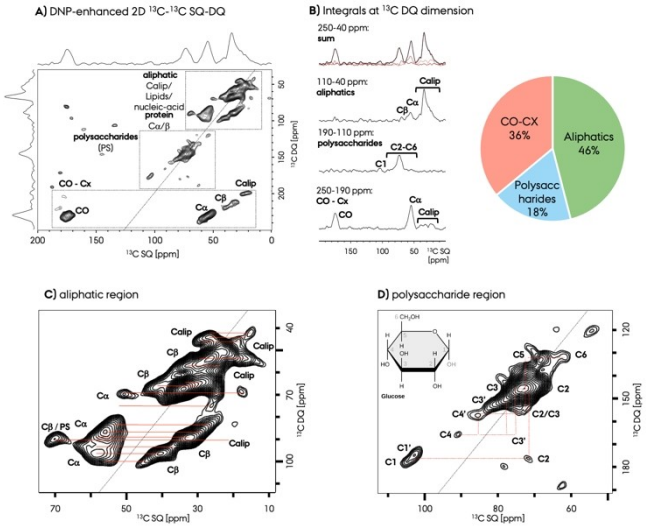

Figure 6. A) DNP-enhanced 2D ^{13}C-^{13}C refocused dipolar INADEQUATE SQ-DQ ssNMR spectrum of natural abundance native wet bacterial biofilm. 100–1500 µs CP contact times were utilized. B) 1D slices extracted between specific DQ chemical shift intervals, corresponding to the CO-Cx, polysaccharide and aliphatic (from protein, lipid, nucleic acid, and so on) chemical shift values. These 1D spectra highlights the potential of 2D ssNMR and results in the non-overlapped signals in 1000 min (~17 h) (3.3 s×288 scans×64 t_1 increment). The zoom out regions for the C) aliphatic and D) polysaccharide areas shown in A.

DNP Facilitates Resonance Assignment by 2D ssNMR Correlation Spectra

The 2D ssNMR spectrum increases spectral resolution, facilitates resonance identification, and is crucial for quantitative analysis in regions with significant spectral overlap. The DNP sensitivity enhancement (ε:~75) enabled the acquisition of 2D DNP ssNMR spectra at natural abundance. Using CP-based methods, we recorded 2D ^{1}H-^{13}C spectra in 18/36 minutes (Figure 5A,B), a 2D ^{1}H-^{15}N spectrum in 90 minutes (Figure 5C), and a 2D ^{13}C-^{13}C spectrum in ~17 hours (Figure 6). In contrast, the conventional room temperature 2D ^{13}C-^{13}C ssNMR spectrum did not produce any cross peaks even after ~40 hours (Figure S6). A low-efficiency 2D ^{13}C-^{13}C single-quantum–double-quantum (SQ-DQ) experiment using ~50 mg of dry, unlabeled biofilm sample was successfully recorded within a day. However, obtaining this spectrum from a wet biofilm was not feasible due to significantly lower efficient rotor packing efficiency and reduced sensitivity.

2D DNP ssNMR spectra, with the additional proton chemical shift dimension, provide detailed insights into tentative resonance assignments, Figure 5. Different proton chemical sites, marked with dashed lines, correspond to components within the biofilm, including protons from amides, aromatics, nucleic acids, sugar rings, and aliphatics. These signals highlights interactions among biofilm components such as polysaccharides, lipids, and the cell wall. A comparison of the short and long CP contact time 2D ^{1}H-^{13}C spectra reveals spatial proximities between biofilm components, Figure 5A,B. For example, the aromatic signals at ~130 ppm ^{13}C chemical shift correlate with a proton signal at ~6.5 ppm at short CP contact time of 100 µs, Figure 5A. At longer CP contact time of 1500 µs, Figure 5B, this peak shows an additional correlation to a protein aliphatic proton but not to a polysaccharide proton, suggesting that the aromatic sites are not in close proximity to biofilm polysaccharides. Furthermore, the absence of amide proton correlation with any anomeric polysaccharide peak supports spatial segregation between these components.

Evidence for nucleic acid signals is present in both 1D ^{13}C and 2D ^{1}H-^{13}C DNP ssNMR spectra. In the 1D ^{13}C spectrum, the resonance at ~93.8 ppm is attributed to a nucleic acid carbon, correlating with a proton chemical shift at ~5 ppm in the 2D ^{1}H-^{13}C spectra recorded at both short and long CP contact times. This 5 ppm proton resonance does not correlate with any polysaccharide, aromatic or protein Cα chemical shift, supporting its tentative assignment to nucleic acids. Additionally, ^{15}N signals above 140 ppm and a ^{13}C chemical shift at 157.7 ppm which correlates with proton peaks at 5 and 6.7 ppm in the 2D spectrum recorded at longer CP contact times, further confirm the presence of nucleic acids in the biofilm.

Finally, the 2D ^{13}C-^{13}C SQ-DQ spectrum, Figure 6A, resolves resonances from the overlapped regions of the 1D ^{13}C spectrum, Figure 3A. Three distinct chemical shift regions are identified, Figure 6A,B: protein (aliphatic and Cα)/lipid/nucleic-acid, polysaccharide and CO. These regions enable the quantitative determination of biofilm components. The aliphatic and carbohydrate regions are further expanded in Figure 6C,D. Tentative resonance assignments were made using the CCMRD carbohydrate and BMRB protein databases.[13k]

Conclusion

We employed high-sensitivity DNP-enhanced ssNMR to characterize the chemical structure and composition of native *P. fluorescens* colony biofilms. For the first time, we demonstrated 2D DNP ssNMR spectra of a complex native bacterial biofilm, enabling the rapid detection of signals from structural components such as polysaccharides, proteins, and other biofilm constituents. Our results highlight the potential of DNP ssNMR as a quantitative tool to simultaneously observe signals from rigid and mobile fractions. This includes recording a low-efficiency 2D ^{13}C-^{13}C spectrum on natural-abundance biofilm via DNP hyperpolarization, analyzing intact native biofilms without chemical extraction or isotope-labelling, characterizing biofilms at natural water content. Furthermore, sensitivity was further increased using dry biofilm samples, allowing for the identification and quantification of biofilm components.

1D DNP ssNMR enabled over a 1000-fold faster detection of $^{13}C/^{15}N$ signals. Homogeneous radical distribution within the biofilm sample facilitated quantitative determination of resonances and the relative abundance of biofilm components. Using ^{15}N DNP ssNMR combined with 2D results, we quantified the extracellular matrix (ECM) relative to bacterial cell-wall components within the biofilm. Additionally, $^{13}C/^{15}N$ signals specific to extracellular DNA (eDNA) was observed. Higher-dimensionality (nD) spectra, including $^{1}H/^{13}C$ second chemical-shift dimensions, improved resolution and facilitated signal identification. Cross-peak patterns in the 2D DNP ssNMR spectra also revealed the spatial segregation of ECM components within the biofilm.

These findings not only demonstrate the technical feasibility of DNP ssNMR for ultrafast analyzing diverse biofilm components, but also establishes a foundation for future biofilm studies. However, we acknowledge that quantifying biofilm components via DNP ssNMR may present challenges, requiring further refinement of sample preparation protocols tailored to specific systems. The use of isotope labeling may provide an alternative strategy for 2D/3D DNP ssNMR experiments, although it is not applicable to patient-derived samples. By introducing high-sensitivity and high-throughput structural characterization, our results aim to advance biofilm structural analysis and contribute to a deeper understanding of these complex biological systems.

Supporting Information

Experimental details and Figures SI1–6 are given. Supporting Information contains references #32–37.

Acknowledgements

UA acknowledges financial support from University of Pittsburgh startup funding and the high-field NMR and Electron Microscopy infrastructure at the Structural Biology Department, School of Medicine, University of Pittsburgh. WK was supported by funding from the National Institute of General Medical Sciences of the NIH 1R15GM132856. The National High Magnetic Field laboratory (NHMFL) is funded by the National Science Foundation Division of Materials Research (DMR-1644779 and DMR-2128556) and the State of Florida. A portion of this work was supported by the NIH P41 GM122698 and RM1-GM148766. F.J.S. acknowledges support from a postdoctoral scholar award from the Provost's Office at Florida State University.

Conflict of Interest

The authors declare no conflict of interest.

Keywords: MAS DNP ssNMR · hyperpolarized NMR · bacterial colony biofilm · *Pseudomonas fluorescens* · biofilm composition

[1] E. K. Perry, M. W. Tan, *Front. Cell. Infect. Microbiol.* **2023**, *13*.
[2] a) M. F. Gebbink, D. Claessen, B. Bouma, L. Dijkhuizen, H. A. Wosten, *Nat. Rev. Microbiol.* **2005**, *3*, 333–341; b) U. Akbey, M. Andreasen, *Chem. Sci.* **2022**, *13*, 6457–6477.
[3] a) H. Ceri, M. E. Olson, C. Stremick, R. R. Read, D. Morck, A. Buret, *J. Clin. Microbiol.* **1999**, *37*, 1771–1776; b) K. Lewis, *Antimicrob. Agents Chemother.* **2001**, *45*, 999–1007.
[4] C. J. Murray, K. S. Ikuta, F. Sharara, L. Swetschinski, G. R. Aguilar, A. Gray, C. Han, C. Bisignano, P. Rao, E. Wool, *Lancet* **2022**.
[5] L. Dieltjens, K. Appermans, M. Lissens, B. Lories, W. Kim, E. V. Van der Eycken, K. R. Foster, H. P. Steenackers, *Nat. Commun.* **2020**, *11*.
[6] L. Karygianni, Z. Ren, H. Koo, T. Thurnheer, *Trends Microbiol.* **2020**, *28*, 668–681.
[7] D. Romero, C. Aguilar, R. Losick, R. Kolter, *Proc. Natl. Acad. Sci. U.S.A.* **2010**, *107*, 2230–2234.
[8] a) A. Diehl, Y. Roske, L. Ball, A. Chowdhury, M. Hiller, N. Moliere, R. Kramer, D. Stoppler, C. L. Worth, B. Schlegel, M. Leidert, N. Cremer, N. Erdmann, D. Lopez, H. Stephanowitz, E. Krause, B. J. van Rossum, P. Schmieder, U. Heinemann, K. Turgay, U. Akbey, H. Oschkinat, *Proc. Natl. Acad. Sci. U.S.A.* **2018**, *115*, 3237–3242; b) J. Bohning, M. Ghrayeb, C. Pedebos, D. K. Abbas, S. Khalid, L. Chai, T. A. M. Bharat, *Nat. Commun.* **2022**, *13*; c) M. Sleutel, B. Pradhan, A. N. Volkov, H. Remaut, *Nat. Commun.* **2023**, *14*; d) F. Bu, R. Dee Derek, B. Liu, *mBio* **2024**, *15*, e00419–00424; e) K. H. Hansen, C. H. Byeon, Q. Liu, T. Drace, T. Boesen, J. F. Conway, M. Andreasen, Ü. Akbey, *Proc. Natl. Acad. Sci.* **2024**, *121*, e2406775121.
[9] a) H. C. Flemming, J. Wingender, *Nat. Rev. Microbiol.* **2010**, *8*, 623–633; b) E. Blanco-Romero, D. Garrido-Sanz, R. Rivilla, M. Redondo-Nieto, M. Martin, *Microorganisms* **2020**, *8*; c) H.-C. Flemming, E. D. van Hullebusch, T. R. Neu, P. H. Nielsen, T. Seviour, P. Stoodley, J. Wingender, S. Wuertz, *Nat. Rev. Microbiol.* **2023**, *21*, 70–86.
[10] J. M. Plitzko, B. Schuler, P. Selenko, *Curr. Opin. Struct. Biol.* **2017**, *46*, 110–121.
[11] a) M. D. Tuttle, G. Comellas, A. J. Nieuwkoop, D. J. Covell, D. A. Berthold, K. D. Kloepper, J. M. Courtney, J. K. Kim, A. M. Barclay, A. Kendall, W. Wan, G. Stubbs, C. D. Schwieters, V. M. Y. Lee, J. M. George, C. M. Rienstra, *Nat. Struct. Mol. Biol.* **2016**, *23*, 409–415; b) S. Asano, B. D. Engel, W. Baumeister, *J. Mol. Biol.* **2016**, *428*, 332–343; c) L. A. Earl, V. Falconieri, S. Subramaniam, *Curr. Opin. Microbiol.* **2018**,

43, 199–207; d) S. Narasimhan, G. E. Folkers, M. Baldus, *Chempluschem* **2020**, *85*, 760–768.
[12] L. Hall-Stoodley, K. S. McCoy, *Front. Cell. Infect. Microbiol.* **2022**, *12*.
[13] a) M. L. Mak-Jurkauskas, V. S. Bajaj, M. K. Hornstein, M. Belenky, R. G. Griffin, J. Herzfeld, *Proc. Natl. Acad. Sci. U.S. A.* **2008**, *105*, 883–888; b) V. S. Bajaj, M. L. Mak-Jurkauskas, M. Belenky, J. Herzfeld, R. G. Griffin, *Proc. Natl. Acad. Sci. U.S.A.* **2009**, *106*, 9244–9249; c) U. Akbey, W. T. Franks, A. Linden, S. Lange, R. G. Griffin, B. J. van Rossum, H. Oschkinat, *Angew. Chem. Int. Ed.* **2010**, *49*, 7803–7806; d) K. K. Frederick, V. K. Michaelis, B. Corzilius, T. C. Ong, A. C. Jacavone, R. G. Griffin, S. Lindquist, *Cell* **2015**, *163*, 620–628; e) S. Lange, W. T. Franks, N. Rajagopalan, K. Doring, M. A. Geiger, A. Linden, B. J. van Rossum, G. Kramer, B. Bukau, H. Oschkinat, *Sci. Adv.* **2016**, *2*; f) M. R. Elkins, I. V. Sergeyev, M. Hong, *J. Am. Chem. Soc.* **2018**, *140*, 15437–15449; g) K. Jaudzems, T. Polenova, G. Pintacuda, H. Oschkinat, A. Lesage, *J. Struct. Biol.* **2019**, *206*, 90–98; h) K. K. Frederick, *Biophys. J.* **2019**, *116*, 203A–203A; i) R. Ghosh, Y. L. Xiao, J. Kragelj, K. K. Frederick, *J. Am. Chem. Soc.* **2021**, *143*, 18454–18466; j) W. Y. Chow, G. De Paepe, S. Hediger, *Chem. Rev.* **2022**, *122*, 9795–9847; k) N. Ghassemi, A. Poulhazan, F. Deligey, F. Mentink-Vigier, I. Marcotte, T. Wang, *Chem. Rev.* **2022**, *122*, 10036–10086.
[14] a) C. Reichhardt, L. M. Joubert, K. V. Clemons, D. A. Stevens, L. Cegelski, *Med. Mycol.* **2019**, *57*, S239–S244; b) J. Jeffries, W. Thongsomboon, J. A. Visser, K. Enriquez, D. Yager, L. Cegelski, *Biopolymers* **2021**, *112*.
[15] a) L. K. Jennings, J. E. Dreifus, C. Reichhardt, K. M. Storek, P. R. Secor, D. J. Wozniak, K. B. Hisert, M. R. Parsek, *Cell Rep.* **2021**, *34*; b) C. Reichhardt, J. C. N. Fong, F. Yildiz, L. Cegelski, *Biochim. Biophys. Acta Biomembr.* **2015**, *1848*, 378–383.
[16] a) X. Kang, A. Kirui, M. C. D. Widanage, F. Mentink-Vigier, D. J. Cosgrove, T. Wang, *Nat. Commun.* **2019**, *10*; b) A. Kirui, W. C. Zhao, F. Deligey, H. Yang, X. Kang, F. Mentink-Vigier, T. Wang, *Nat. Commun.* **2022**, *13*.
[17] a) R. Nygaard, J. A. H. Romaniuk, D. M. Rice, L. Cegelski, *Biophys. J.* **2015**, *108*, 1380–1389; b) C. Laguri, A. Silipo, A. M. Martorana, P. Schanda, R. Marchetti, A. Polissi, A. Molinaro, J. P. Simorre, *ACS Chem. Biol.* **2018**, *13*, 2106–2113; c) C. Bougault, I. Ayala, W. Vollmer, J. P. Simorre, P. Schanda, *J. Struct. Biol.* **2019**, *206*, 66–72; d) A. Vallet, I. Ayala, B. Perrone, A. Hassan, J.-P. Simorre, C. Bougault, P. Schanda, *J. Magn. Reson.* **2024**, *364*, 107708.
[18] P. Phyo, M. Hong, *J. Biomol. NMR* **2019**, *73*, 661–674.
[19] a) C.-H. Byeon, K. H. Hansen, W. DePas, Ü. Akbey, *bioRxiv* **2024**, 2024.2005.2028.596255; b) C.-H. Byeon, T. Kinney, H. Saricayir, S. Srinivasa, M. K. Wells, W. Kim, Ü. Akbey, *J. Magn. Reson.* **2023**, *357*, 107587.
[20] a) H. Takahashi, I. Ayala, M. Bardet, G. De Paepe, J. P. Simorre, S. Hediger, *J. Am. Chem. Soc.* **2013**, *135*, 5105–5110; b) R. Bastos, I. Marín-Montesinos, S. S. Ferreira, F. Mentink-Vigier, M. Sardo, L. Mafra, M. A. Coimbra, E. Coelho, *Carbohydr. Polym.* **2024**, *324*, 121475.
[21] a) W. Kim, F. Racimo, J. Schluter, S. B. Levy, K. R. Foster, *Proc. Natl. Acad. Sci. U.S.A.* **2014**, *111*, E1639–E1647; b) W. Kim, S. B. Levy, K. R. Foster, *Nat. Commun.* **2016**, *7*; c) A. F. Evans, M. K. Wells, J. Denk, W. Mazza, R. Santos, A. Delprince, W. Kim, *J. Bacteriol.* **2022**, *204*; d) C. Kessler, W. Kim, *Msystems* **2022**, *7*.
[22] a) X. Kang, A. Kirui, A. Muszynski, M. C. D. Widanage, A. Chen, P. Azadi, P. Wang, F. Mentink-Vigier, T. Wang, *Nat. Commun.* **2018**, *9*; b) A. Bertarello, P. Berruyer, M. Artelsmair, C. S. Elmore, S. Heydarkhan-Hagvall, M. Schade, E. Chiarparin, S. Schantz, L. Emsley, *J. Am. Chem. Soc.* **2022**, *144*, 6734–6741.
[23] a) Y. L. Xiao, R. Ghosh, K. K. Frederick, *Front. Mol. Biosci.* **2022**, *8*; b) K. Singewald, M. J. Lawless, S. Saxena, *J. Magn. Reson.* **2019**, *299*, 21–27.
[24] a) F. Mentink-Vigier, I. Marin-Montesinos, A. P. Jagtap, T. Halbritter, J. van Tol, S. Hediger, D. Lee, S. T. Sigurdsson, G. De Paepe, *J. Am. Chem. Soc.* **2018**, *140*, 11013–11019; b) S. Chatterjee, A. Venkatesh, S. T. Sigurdsson, F. Mentink-Vigier, *J. Phys. Chem. Lett.* **2024**, *15*, 2160–2168.
[25] F. Mentink-Vigier, S. Paul, D. Lee, A. Feintuch, S. Hediger, S. Vega, G. De Paepe, *Phys. Chem. Chem. Phys.* **2015**, *17*, 21824–21836.
[26] L. Cegelski, D. Stueber, A. K. Mehta, D. W. Kulp, P. H. Axelsen, J. Schaefer, *J. Mol. Biol.* **2006**, *357*, 1253.
[27] S. G. J. van Meerten, W. M. J. Franssen, A. P. M. Kentgens, *J. Magn. Reson.* **2019**, *301*, 56–66.
[28] a) G. J. Patti, S. J. Kim, J. Schaefer, *Biochemistry* **2008**, *47*, 8378–8385; b) J. A. H. Romaniuk, L. Cegelski, *Philos. Trans. R. Soc. B-Biol. Sci.* **2015**, *370*; c) X. Kang, W. C. Zhao, M. D. C. Widanage, A. Kirui, U. Ozdenvar, T. Wang, *J. Biomol. NMR* **2020**, *74*, 239–245.
[29] J. A. Romaniuk, L. Cegelski, *Biophys. J.* **2018**, *114*, 158A–158A.
[30] J. A. H. Romaniuk, L. Cegelski, *Biochemistry* **2018**, *57*, 3966–3975.
[31] C. Reichhardt, J. A. G. Ferreira, L. M. Joubert, K. V. Clemons, D. A. Stevens, L. Cegelski, *Eukaryot. Cell* **2015**, *14*, 1064–1072.
[32] W. P. J. Smith, Y. Davit, J. M. Osborne, W. Kim, K. R. Foster, J. M. Pitt-Francis, *Proc. Natl. Acad. Sci. U.S.A.* **2017**, *114*, E280–E286.
[33] R. Harrabi, T. Halbritter, F. Aussenac, O. Dakhlaoui, J. van Tol, K. K. Damodaran, D. Lee, S. Paul, S. Hediger, F. Mentink-Vigier, S. T. Sigurdsson, G. De Paepe, *Angew. Chem. Int. Ed.* **2022**, *61*.
[34] D. S. Wishart, C. G. Bigam, A. Holm, R. S. Hodges, B. D. Sykes, *J. Biomol. NMR* **1995**, *5*, 67–81.
[35] T. V. Can, J. E. McKay, R. T. Weber, C. Yang, T. Dubroca, J. van Tol, S. Hill, R. G. Griffin, *J. Phys. Chem. Lett.* **2018**, *9*, 3187–3192.
[36] A. Bielecki, A. C. Kolbert, M. H. Levitt, *Chem. Phys. Lett.* **1989**, *155*, 341–346.
[37] M. Hohwy, H. J. Jakobsen, M. Edén, M. H. Levitt, N. C. Nielsen, *J. Chem. Phys.* **1998**, *108*, 2686–2694.

Manuscript received: September 22, 2024
Revised manuscript received: December 27, 2024
Accepted manuscript online: January 7, 2025
Version of record online: ■■, ■■

Research Article

NMR Spectroscopy

C.-H. Byeon, T. Kinney, H. Saricayir, K. Holst Hansen, F. J. Scott, S. Srinivasa, M. K. Wells, F. Mentink-Vigier, W. Kim, Ü. Akbey* _____ **e202418146**

Ultrasensitive Characterization of Native Bacterial Biofilms via Dynamic Nuclear Polarization-Enhanced Solid-State NMR

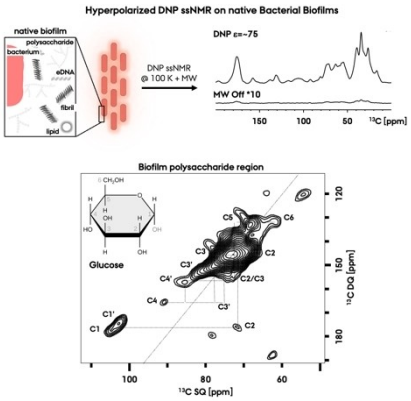

Bacterial biofilms cause persistent infections and contribute to antimicrobial resistance. We utilized for the first time hyperpolarized DNP solid-state NMR to structurally characterize native bacterial biofilm. We collected 1D/2D spectra within seconds/minutes and detected polysaccharide, protein and other signals. These structural information will boost structure-guided approaches for combating biofilm-forming microbes.